Article

On the usage of tapered undulators in the measurement of interference in the intensity-dependent electron mass shift

Maksim Valialshchikov [1,†], Marcel Ruijter [2,3], Sergey Rykovanov [1,†]

1 High Performance Computing and Big Data Laboratory, Skolkovo Institute of Science and Technology, Moscow, Russia
2 INFN, Sezione di Roma and Dipartimento di Fisica, University of Rome "La Sapienza", Piazzale Aldo Moro 5, 00185 Rome, Italy
3 INFN-Sezione di Milano, via Celoria 16, 20133, Milano, Italy
* Correspondence: s.rykovanov@skoltech.ru
† These authors contributed equally to this work.

Abstract: In nonlinear Thomson scattering the main emission line and its harmonics form the band-like structure due to the laser pulse shape induced ponderomotive broadening. We propose to use tapered undulators to mimic Thomson scattering and measure the intensity-dependent electron mass shift experimentally. We also numerically show, that the effect is observable for realistic electron beams like in DESY or SKIF.

Keywords: Thomson scattering, Compton scattering, synchrotron radiation, undulator radiation

Citation: Valialshchikov, M.; Ruijter, M., Rykovanov, S. On the usage of tapered undulators in the measurement of interference in the intensity-dependent electron mass shift. *Crystals* **2021**, *1*, 0. https://doi.org/

Received:
Accepted:
Published:

1. Introduction

An electron passing through a laser field emits radiation, which frequency is red-shifted depending on the laser field strength. This frequency shift is attributed by some to the intensity-dependent increase of the electron's effective mass [1,2]. This effect is best seen in high-intensity laser pulses with a temporal profile, which leads to significant non-linear broadening [3–8]. There are some techniques to alleviate ponderomotive broadening, for instance, using laser pulses with flat-top profiles [4] or laser chirping techniques, where the laser frequency changes non-linearly to repeat the change of temporal envelope [7,9–11]. Recently, it was theoretically shown that it is possible to use only linear chirp to avoid ponderomotive broadening for high laser field intensities [12,13]. Also, it was proposed to use laser pulses with temporally varying polarization to avoid ponderomotive broadening in the harmonics spectrum [14]. However, with ponderomotive broadening the main Thomson line as well as its harmonics form a characteristic interference pattern which, to the best of our knowledge, has not been measured experimentally so far.

Strong laser scattering systems typically have $\omega_0 \sim 1.55$ eV, which produces MeV photons when scattering off the ultrarelativistic electron beams ($\gamma \sim 500$). Current detector technology is unable to resolve such high-energy radiation spectrum with good quality, that is why we propose to mimic the Thomson scattering process with tapered undulators by constructing an appropriate electromagnetic field profile. Typical undulator frequency is several orders of magnitude smaller than that of a strong laser, namely, undulator wavelength $\lambda_u \sim 1$ cm corresponds to $\omega_u \sim 1.24 \times 10^{-4}$eV and the radiation spectrum lies in the keV region. When $\gamma \gg 1$ the Thomson and undulator radiation are essentially the same up to the scaling factor of 2 (in Thomson scattering the initial laser frequency is upscaled with $4\gamma^2$ while in undulator - by $2\gamma^2$). Taking this into account, it is appropriate to mimic one phenomenon through another.

In this paper, we show using numerical simulations of the nonlinear Thomson scattering process that it is possible to measure the band-like structure of the main emission line as well as its harmonics which is present due to the laser pulse shape

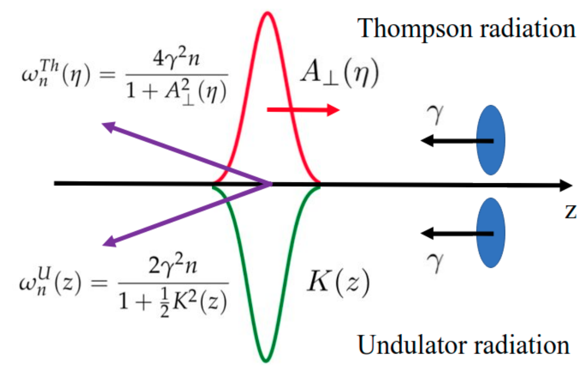

Figure 1. Sketch of (Top) Thomson radiation and (Bottom) undulator radiation problem settings. Blue ellipses correspond to electron bunches propagating in $-z$ direction. In Thomson scattering a laser pulse with a temporal envelope (red) is counter-propagating an electron bunch, while a tapered undulator (green) is at rest. Backscattered radiation is depicted by purple arrows along with expressions for emitted harmonic frequencies. $K(z) = K\,g(z)$, for linear polarization $A_\perp(\eta) = \frac{1}{2}\,a_0\,g(\eta)$, $\eta = t - z$ is the light-front time, n is an odd integer standing for harmonic number. The emitted frequencies differ only by a scaling factor of 2.

induced ponderomotive broadening (called by others the intensity-dependent electron mass shift). We also propose a concept of an experiment for that purpose: by joining two tapered undulators it is possible to form a field configuration, from which the radiation spectrum would be the same as the Thomson spectrum from the laser pulse with a "roof-like" temporal envelope.

Throughout the paper, we use $\hbar = c = 1$ units system, dimensionless spacetime $(x\omega_F \to x)$, and energy $(\omega/\omega_F \to \omega)$ variables by rescaling with the frequency of the field $\omega_F = 2\pi c/\lambda_F$, where λ_F is either the undulator (λ_u) - or the laser pulse wavelength (λ_l). The dimensionless undulator (laser) strength parameter is $K = eB_0\lambda_u/2\pi m$ $(= a_0 = eA/m)$, where B_0 is the amplitude of the magnetic field, A is the amplitude of the vector potential, e, m is the absolute value of electron charge and electron mass respectively. We will use K and a_0 interchangeably. We consider the case of ultrarelativistic electrons $\gamma \gg 1$ when the undulator slippage is negligible. Also, we are interested in moderately strong $K \sim 1$ and relatively short undulators when the nonlinear effects are essential and the energy loss of an electron bunch is very small.

2. Methods

In our problem setting, electrons are moving in the $-z$ direction, counter-propagating a laser pulse with a temporal envelope, which is analogous to the case when the electron bunch is moving through a tapered undulator at rest (see Figure 1). Throughout the paper, we will use laser pulses with an undulator temporal envelope

$$g(z) = 1 - \frac{2|z|}{\tau}\Delta,\ z \in [-\frac{\tau}{2}, \frac{\tau}{2}], \tag{1}$$

where $\tau = 2\pi N$ is the laser pulse length, N stands for the number of cycles, $\Delta \in [0, 1]$ is the tapering rate. This temporal envelope corresponds to the tapered undulator field $\mathbf{B} = (0, B_0\,g(z)\cos z, 0)$, which may be achieved by "joining" positively (K is increasing) and negatively tapered undulators together. $\Delta = 1$ (triangle envelope) is a limit case of examined function corresponding to an infinite initial transverse gap between magnets, while $\Delta = 0$ (rectangular pulse) corresponds to a regular (untapered) undulator.

The spectrum is obtained by numerical calculation of the following integral [15]

$$\frac{d^2 I}{d\omega d\Omega} = \frac{\omega^2}{4\pi^2}\left|\int_{-\infty}^{\infty} d\eta\ \mathbf{n}\times[\mathbf{n}\times\mathbf{u}]\,e^{i\omega(\eta + z - \mathbf{nr})}\right|^2, \tag{2}$$

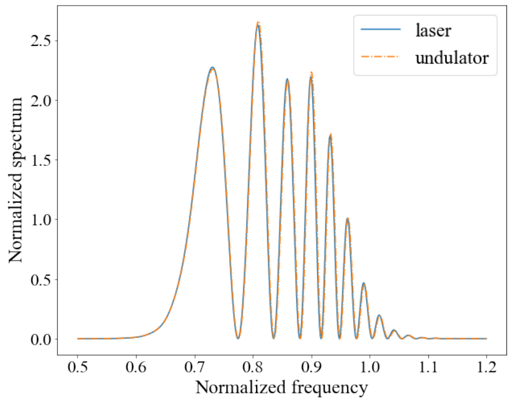

Figure 2. Backscattered spectrum from one electron ($\gamma = 1000$) off a laser pulse with a triangular envelope and spectrum from one electron moving in a tapered undulator. Frequency is normalized by $4\gamma^2$ for laser pulse case and by $2\gamma^2$ for undulator case. Laser pulse parameters: $K = 1.0$, $N = 40$. The emitted spectra coincide up to the frequency scaling factor.

where Ω is the solid angle, $\mathbf{n}$ is the unit vector pointing from origin to the observation point, $\mathbf{u}, \mathbf{r}$ is the vector part of electron 4-velocity and 3-coordinate respectively. Considering this equation as the Fourier transform in retarded time one may use Fast Fourier Transform to efficiently calculate it [16]. Theoretical classical estimates of backscattered spectrum for symmetric laser pulse shapes could be found in [16]. From Eq. 2 the Thomson and undulator emitted harmonic frequencies can be found and are given by

$$\omega_n^{Th}(\eta) = \frac{4\gamma^2 n}{1 + A_\perp^2(\eta)}, \; \omega_n^{U}(z) = \frac{2\gamma^2 n}{1 + \frac{1}{2}K^2(z)}, \tag{3}$$

where $A_\perp(\eta) = \frac{1}{2}\, a_0\, g(\eta)$ is the amplitude of a linearly polarized laser field vector potential, $\eta = t - z$ is the light-front time, n is an odd integer standing for harmonic number, $K(z) = K\, g(z)$.

All figures in the Results section were obtained through numerical simulations. Scattering from one electron was simulated via the aforementioned Fourier method, while simulations involving electron beams were obtained with the code VDSR [17].

3. Results

In the Results section, we present figures and their discussion which is organized in the following way. Scattering from one electron is presented in Section 3.1, where we numerically show 1) the similarity between the emission spectra from Thomson radiation and undulator radiation, 2) the dependence of the interference pattern on the tapering rate, 3) the dependence of the interference pattern on the laser strength and length (K, N). Scattering from a realistic electron beam is discussed in Section 3.2, namely, 1) how electron beam's angular and energy divergence affects the visibility of the interference pattern, 2) how increasing laser pulse strength leads to stronger nonlinear effects and how to observe the band-like structure in the harmonics spectrum, 3) how larger tapering rates result in a broader interference pattern.

3.1. *Scattering from one electron*

Figure 2 shows backscattered spectra from one electron ($\gamma = 1000$) off a laser pulse ($K = 1, N = 40$) with a triangular temporal envelope and tapered undulator ($\Delta = 1$). As it was expected, taking into account different frequency normalization, for ultra-relativistic electrons the emitted spectra are the same.

In Figure 3 the normalized vector potentials and corresponding backscattered spectra from one electron off a laser pulse with an undulator temporal envelope for various tapering rates ($\Delta = 1$, 0.3, 0) are shown. The field intensity ($K = 1.0, N = 20$)

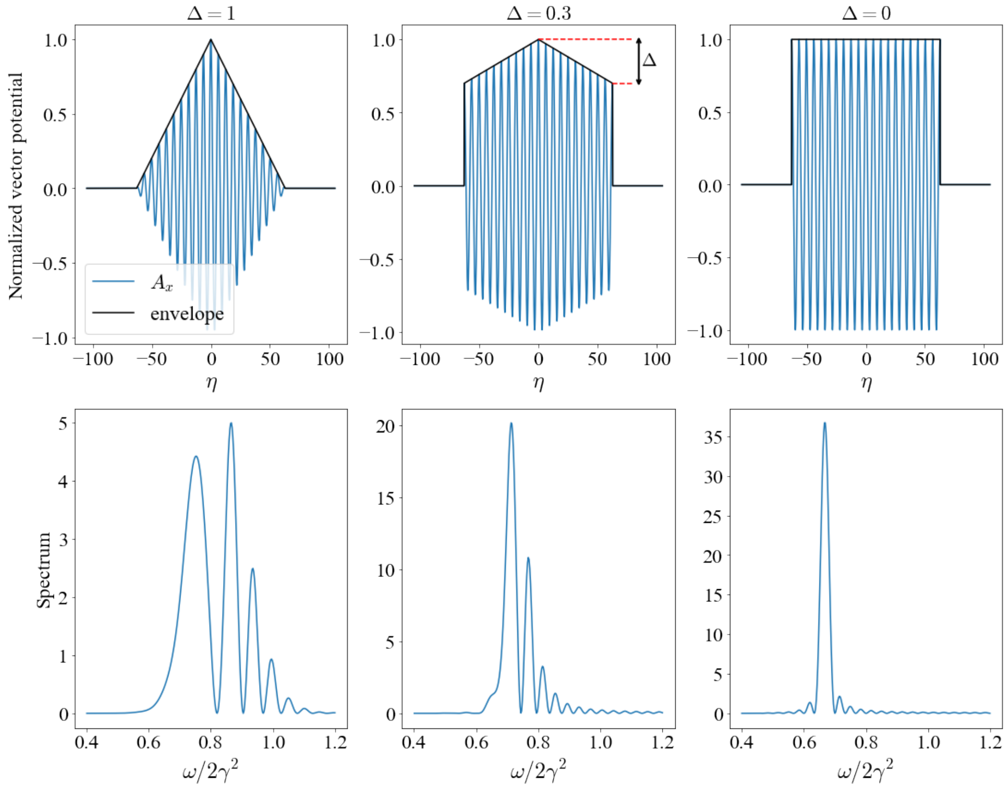

Figure 3. (Top) Normalized vector potential of a laser pulse with an undulator temporal envelope. (Bottom) Corresponding backscattered spectrum from one electron. Laser pulse parameters: $K = 1.0$, $N = 20$. Presented tapering rates: $\Delta = 1$, 0.3, 0. For larger tapering rates the spectrum is broadened more and one may observe stronger interference pattern due to the larger laser field amplitude variation.

is, on the one hand, large enough for the interference pattern from ponderomotive broadening to be distinctly seen and, on the other hand, small enough so the harmonics do not overlap with each other. As it was already mentioned, the main emission line for typical undulators resides in the keV range, therefore, the spectrum could be resolved in detail by modern detectors and one could measure this band-like structure in the experiment. We are interested in the band-like interference pattern, which is broader with larger Δ (Figure 3). Typical tapered undulators for FEL applications have relatively low tapering rates around $1-5\%$ or less [18,19], for which the interference pattern is quite small, while for our purposes strongly tapered undulators are needed. Therefore, we make scan simulations with a triangle envelope for different laser pulse and electron beam parameters and then for a selected set of parameters several tapering rates are modeled.

We examined how the interference pattern behaves when varying tapering rates for fixed laser pulse strength and length. Now, to give the intuition of how the interference pattern changes with laser pulse strength and length, let us fix the tapering rate. Figure 4 shows the main emission line in the backscattered spectrum off a laser pulse with the undulator temporal envelope with tapering rate $\Delta = 0.7$ for several laser pulse strength and length. It could be seen that increasing laser pulse strength leads to a broader interference pattern due to the higher redshift of the main emission line for stronger nonlinear effects. Also, increasing the length of the pulse results in a more intense interference pattern and a higher number of sub-peaks due to the increase of the number of constructively interfering points in the electron's trajectory.

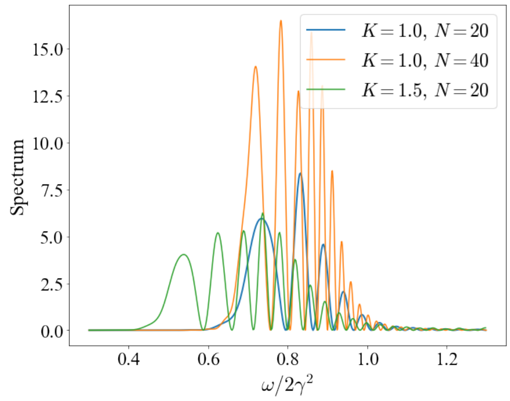

Figure 4. Backscattered spectrum from one electron off a laser pulse with the an undulator temporal envelope with tapering rate $\Delta = 0.7$ for three cases: (blue) $K = 1.0,\ N = 20$, (orange) $K = 1.0,\ N = 40$, (green) $K = 1.5,\ N = 20$. One may see that when increasing laser pulse strength the main emission line is redshifted and the interference pattern becomes broader while increasing the number of cycles in a pulse leads to a more intense interference pattern and a higher number of sub-peaks.

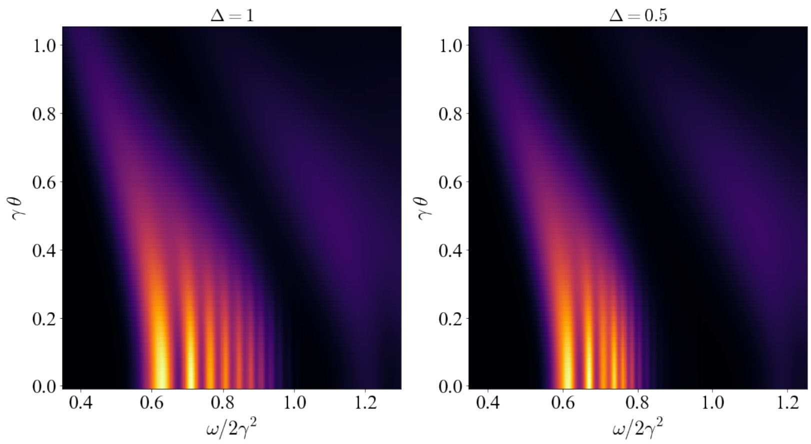

Figure 5. Angular distribution of radiation spectrum from an electron beam: $\gamma = 1000$, $\delta E = 10^{-3}$, $\sigma_p = 0.15$. Laser pulse $K = 1.2$, $N = 40$ with (left) triangular and (right) undulator ($\Delta = 0.5$) temporal envelope. The band-like structure is more visible close to the axis.

3.2. *Scattering from an electron beam*

To investigate how a non-ideal electron beam influences the observability of the band-like structure, we conducted series of numerical simulations for various realistic laser and electron beam parameters. The electron beam is represented with 10^8 electrons, $\gamma = 1000$, energy divergence $\delta E \sim 10^{-3}$ and normalized emittance $\epsilon_n = \sigma_p\,\sigma_r \sim 1.4$ mm mrad where σ_p, σ_r are the angular and radial divergence respectively. Such parameters are similar to electron beams from DESY FLASH [20] and SKIF [21]. The undulator wavelength $\lambda_u = 3$ cm and all transverse beam size effects are negligible. Figure 5 shows the angular distribution of radiation spectrum from an electron beam ($\delta E = 10^{-3}, \sigma_p = 0.15$) off a laser pulse with $K = 1.2, N = 40$ for tapering rates $\Delta = 1,\ 0.5$. Close to the axis, the sub-peaks are distinctly seen, while further off axis they are more blurred. Moreover, for the ideal electron beam only odd harmonics are emitted on-axis while in our case due to the broadening caused by non-ideal beam effects, a part of the 2^{nd} harmonic could be visible on-axis as well. It could also be expected and seen that for larger tapering rate the interference pattern is more distinctly seen and every sub-peak is broader.

For larger energy divergence δE and angular divergence σ_p the interference pattern is less visible due to the larger range of frequencies emitted (Eq. 2). In order to estimate

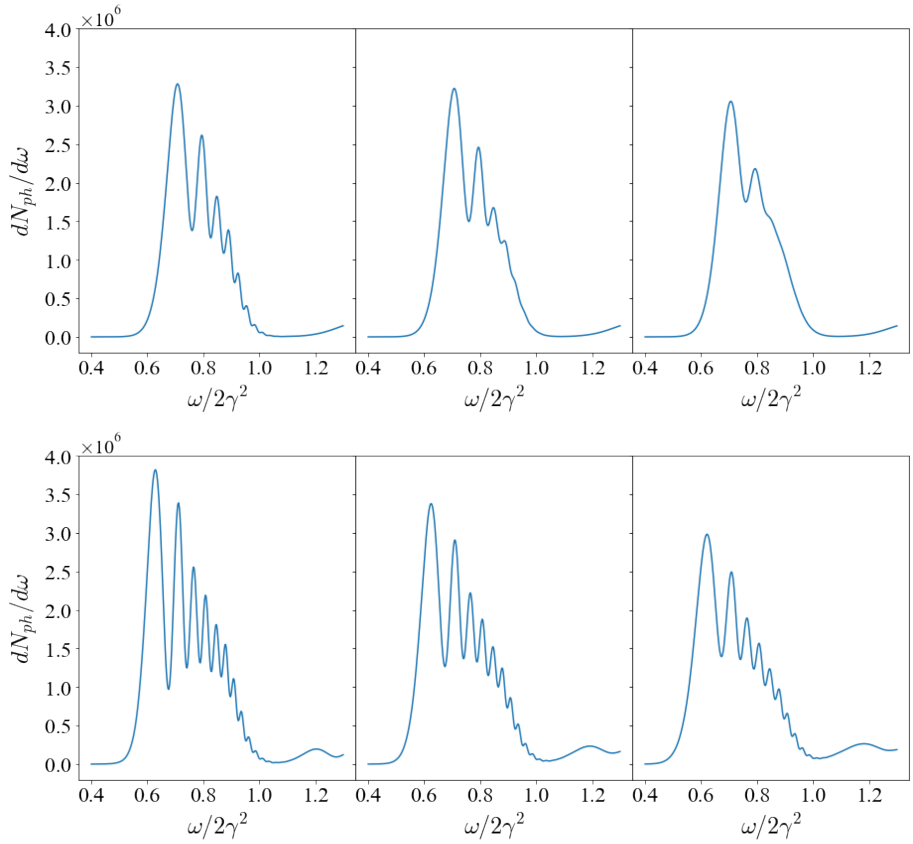

Figure 6. The differential number of photons scattered from a realistic electron beam (10^8 electrons, $\gamma = 1000$) for various electron beam angular (σ_p) and energy (δE) divergence off a laser pulse with a triangular envelope. (Top) $K = 1$, $N = 40$, $\sigma_p = 0.15$, δE (left to right): 10^{-3}, $5 \cdot 10^{-3}$, 10^{-2}. (Bottom) $K = 1.2$, $N = 40$, $\delta E = 10^{-3}$, σ_p (left to right): 0.1, 0.15, 0.2. For more ideal electron beam parameters (less energy and angular divergence) the sub-peaks are more distinguishable.

the visibility of band-like structure, we scanned over several values of δE, σ_p while other parameters remained fixed. The top panel of Figure 6 shows the differential number of photons scattered from the electron beam ($\sigma_p = 0.15$) off a triangle laser pulse with $K = 1$, $N = 40$ for different energy divergence $\delta E = 10^{-3}$, $5 \cdot 10^{-3}$, 10^{-2}. The bottom panel of Figure 6 corresponds to a triangle laser pulse with $K = 1.2$, $N = 40$ and various electron beam ($\delta E = 10^{-3}$) angular divergence $\sigma_p = 0.1$, 0.15, 0.2. Number of photons is obtained from the angular spectrum distribution $\frac{d^2 N_{ph}}{d\omega d\Omega} = \alpha \frac{1}{\omega} \frac{d^2 I}{d\omega d\Omega}$, where $\alpha \approx 1/137$ is the fine structure constant, by integration over the polar angle ϕ and collimation angle $\theta_{col} = 0.2/\gamma$. As expected, for greater angular and energy divergence the band-like structure is more smoothed but for the chosen parameters (except $\delta E = 10^{-2}$) the band-structure is still visible.

From Eq. 3 we could see that on axis the main emission line is broadened from $\omega \sim \frac{1}{1+K^2/2}$ up to $\omega \sim 1$. In other words, for larger K the nonlinearity effects are stronger, leading to a broader main emission line and broader harmonics. For large K harmonics may start to overlap due to both ponderomotive broadening and non-ideal electron beam effects. Figure 7 represents results for fixed angular and energy divergence ($\sigma_p = 0.15$, $\delta E = 10^{-3}$) and increasing laser strength $K = 0.8$, 1.0, 1.2. The interference pattern is visible for all cases, and there are more sub-peaks for stronger pulses. The same band-like structure could be observed in harmonics as well, for instance, Figure 8 shows the differential number of photons in the harmonics region for a triangle envelope for two cases: 1) $K = 1$, $\sigma_p = 0.15$, $\theta_{col} = 0.2/\gamma$, 2) $K = 0.8$, $\sigma_p = 0.1$, $\theta_{col} = 0.1/\gamma$. For the first case due to a relatively large collimation angle and non-ideal beam effects even

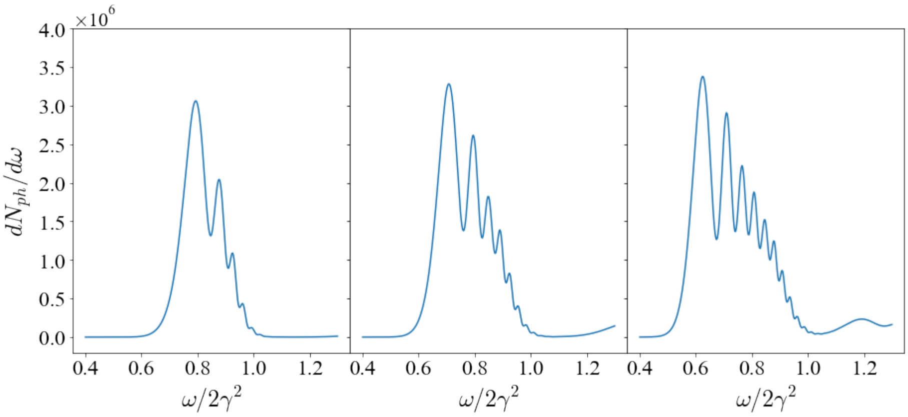

Figure 7. The differential number of photons scattered from a realistic electron beam (10^8 electrons, $\gamma = 1000$, $\delta E = 10^{-3}$, $\sigma_p = 0.15$) off a triangle laser pulse $N = 40$. Laser pulse strength K (left to right): 0.8, 1.0, 1.2. In stronger laser pulses electron's nonlinear response is larger which leads to broader spectrum and more interference sub-peaks.

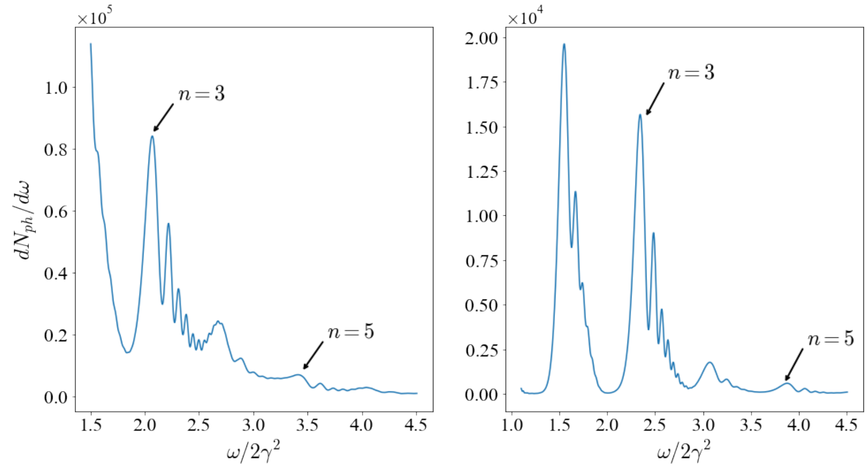

Figure 8. The differential number of photons (harmonics region) scattered from a realistic electron beam (10^8 electrons, $\gamma = 1000$, $\delta E = 10^{-3}$) off a laser pulse with a triangular envelope. (Left) $\sigma_p = 0.15$, $K = 1$, $N = 40$, $\theta_{col} = 0.2/\gamma$, (Right) $\sigma_p = 0.1$, $K = 0.8$, $N = 40$, $\theta_{col} = 0.1/\gamma$. Choosing smaller collimation angles and more ideal electron beam parameters leads to a more visible interference pattern in harmonics.

off-axis harmonics overlap with odd on-axis ones, which spoils the overall picture. Still, we can consider more ideal electron beam parameters and a smaller collimation angle to make the interference pattern more visible.

Now, after we observed the influence of laser pulse and electron beam parameters on the interference pattern, it is interesting to model several tapering rates for some "optimal" parameters to make sure that a distinct band-like structure remains. Figure 9 shows the differential number of photons scattered from a realistic electron beam ($\delta E = 10^{-3}$, $\sigma_p = 0.15$) off a laser pulse ($K = 1.2$, $N = 40$) with various tapering rates $\Delta = 0.4, 0.5, 0.6$. As it was already discussed, for smaller tapering rates the interference is less distinct. Also, stronger tapered pulses contain less energy, therefore the resulting spectrum is less intense. Speaking about experimental observation, for $\Delta = 0.5$, $K = 1.2$, $\lambda_u = 1$ cm and $\gamma = 1000$ the main emission peak is at $\frac{\omega}{2\gamma^2} = 0.6$ ($\lambda \sim 8.6$ nm) and the first subsidiary peak is at $\frac{\omega}{2\gamma^2} = 0.7$ ($\lambda \sim 7.1$ nm). This difference is large enough to be measured experimentally. For larger λ_u or lower γ the difference between these peaks increases, and it is easier to detect the interference pattern.

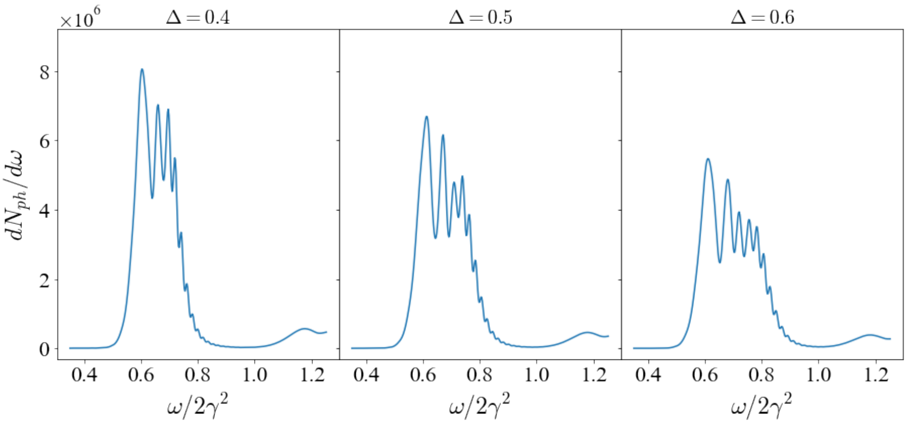

Figure 9. The differential number of photons scattered from a realistic electron beam (10^8 electrons, $\gamma = 1000$, $\delta E = 10^{-3}$, $\sigma_p = 0.15$) off a laser pulse ($K = 1.2$, $N = 40$) with different tapering rates $\Delta = 0.4$, 0.5, 0.6. For large tapering rates the interference pattern is distinct. Lasers with stronger tapering rates contain less energy, the resulting spectrum is less intense.

4. Conclusions

Overall, we proposed to use tapered undulators to mimic Thomson scattering and measure the intensity-dependent electron mass shift experimentally, namely, one may connect positively (K is increasing) and negatively tapered undulators to obtain radiation spectrum similar to Thomson spectrum off a laser pulse with an undulator temporal envelope. Firstly, we conducted series of numerical simulations for triangular temporal envelope (which has the most vivid interference pattern) scanning over the range of laser pulse and electron beam parameters. Secondly, for a chosen set of laser and electron beam parameters, we modeled several cases with different tapering rates to show that for modern realistic electron beam parameters, the effect is not completely smoothed out and still could be distinctly seen in the main emission line for a broad range of parameters. To observe this band-like structure in harmonics, one needs to choose smaller collimation angles and/or more ideal electron beams. Finally, the intensity-dependent electron mass shift can be observed experimentally by measuring the difference in wavelength of the subsidiary peaks. For a tapered undulator $\Delta = 0.5$, $K = 1.2$, $\lambda_u = 1$cm and an electron bunch $\gamma = 1000$, $\epsilon_n = 1.4$ mm mrad the difference is $\Delta\lambda \sim 1$ nm.

Author Contributions: Conceptualization, S. Rykovanov; methodology, S. Rykovanov, M. Valialshchikov; formal analysis, M. Valialshchikov; writing—original draft preparation, M. Valialshchikov; writing—review and editing, M. Valialshchikov, M. Ruijter, S. Rykovanov; supervision, S. Rykovanov. All authors have read and agreed to the published version of the manuscript.

Funding: This research received no external funding.

Acknowledgments: The authors acknowledge the usage of Skoltech CDISE supercomputer "Zhores" [22] for obtaining the numerical results presented in this paper.

Conflicts of Interest: The authors declare no conflict of interest.

References

1. Kibble, T. Mutual refraction of electrons and photons. *Physical Review* **1966**, *150*, 1060.
2. Harvey, C.; Heinzl, T.; Ilderton, A.; Marklund, M. Intensity-dependent electron mass shift in a laser field: existence, universality, and detection. *Physical review letters* **2012**, *109*, 100402.
3. Nedorezov, V.G.; Rykovanov, S.G.; Savel'ev, A.B. Nuclear photonics. Results and prospects. *Physics-Uspekhi, accepted*.
4. Hartemann, F.; Troha, A.; Luhmann Jr, N.; Toffano, Z. Spectral analysis of the nonlinear relativistic Doppler shift in ultrahigh intensity Compton scattering. *Physical Review E* **1996**, *54*, 2956.

5. Hartemann, F.V.; Wu, S.S. Nonlinear brightness optimization in Compton scattering. *Physical review letters* **2013**, *111*, 044801.
6. Heinzl, T.; Seipt, D.; Kämpfer, B. Beam-shape effects in nonlinear Compton and Thomson scattering. *Physical Review A* **2010**, *81*, 022125.
7. Rykovanov, S.; Geddes, C.; Schroeder, C.; Esarey, E.; Leemans, W. Controlling the spectral shape of nonlinear Thomson scattering with proper laser chirping. *Physical Review Accelerators and Beams* **2016**, *19*, 030701.
8. Seipt, D.; Kämpfer, B. Nonlinear Compton scattering of ultrashort intense laser pulses. *Physical Review A* **2011**, *83*, 022101.
9. Ghebregziabher, I.; Shadwick, B.A.; Umstadter, D. Spectral bandwidth reduction of Thomson scattered light by pulse chirping. *Physical Review Special Topics-Accelerators and Beams* **2013**, *16*, 030705.
10. Seipt, D.; Rykovanov, S.; Surzhykov, A.; Fritzsche, S. Narrowband inverse Compton scattering x-ray sources at high laser intensities. *Physical Review A* **2015**, *91*, 033402.
11. Terzić, B.; Deitrick, K.; Hofler, A.S.; Krafft, G.A. Narrow-band emission in Thomson sources operating in the high-field regime. *Physical Review Letters* **2014**, *112*, 074801.
12. Seipt, D.; Kharin, V.Y.; Rykovanov, S.G. Optimizing Laser Pulses for Narrow-Band Inverse Compton Sources in the High-Intensity Regime. *Physical review letters* **2019**, *122*, 204802.
13. Kharin, V.Y.; Seipt, D.; Rykovanov, S.G. Higher-dimensional caustics in nonlinear compton scattering. *Physical review letters* **2018**, *120*, 044802.
14. Valialshchikov, M.; Kharin, V.Y.; Rykovanov, S. Narrow bandwidth gamma comb from nonlinear Compton scattering using the polarization gating technique. *arXiv preprint arXiv:2011.12931* **2020**.
15. Jackson, J.D. Classical electrodynamics, 1999.
16. Kharin, V.Y.; Seipt, D.; Rykovanov, S. Temporal laser-pulse-shape effects in nonlinear Thomson scattering. *Physical Review A* **2016**, *93*, 063801.
17. Chen, M.; Esarey, E.; Geddes, C.; Schroeder, C.; Plateau, G.; Bulanov, S.; Rykovanov, S.; Leemans, W. Modeling classical and quantum radiation from laser-plasma accelerators. *Physical Review Special Topics-Accelerators and Beams* **2013**, *16*, 030701.
18. He-Ting, L.; Fan, G.; Jia-Yu, L.; Qi-Ka, J. Calculation and analysis of the magnetic field of a linearly tapered undulator. *Chinese Physics C* **2015**, *39*, 088101.
19. Fawley, W.M.; Huang, Z.; Kim, K.J.; Vinokurov, N.A. Tapered undulators for SASE FELs. *Nuclear Instruments and Methods in Physics Research Section A: Accelerators, Spectrometers, Detectors and Associated Equipment* **2002**, *483*, 537–541.
20. Faatz, B.; Braune, M.; Hensler, O.; Honkavaara, K.; Kammering, R.; Kuhlmann, M.; Ploenjes, E.; Roensch-Schulenburg, J.; Schneidmiller, E.; Schreiber, S.; others. The FLASH facility: Advanced options for FLASH2 and future perspectives. *Applied Sciences* **2017**, *7*, 1114.
21. Zakharov, B.; Vinokurov, Z.; Rashchenko, S.; Shmakov, A.; Boldyreva, E.; Gromilov, S.; Sukhikh, A.; Komarov, V.; Larichev, Y.; Tsybulya, S.; others. A concept of 1-2 "structural diagnostics" diffraction beamline for "SKIF" synchrotron radiation facility. AIP Conference Proceedings. AIP Publishing LLC, 2020, Vol. 2299, p. 060002.
22. Zacharov, I.; Arslanov, R.; Gunin, M.; Stefonishin, D.; Bykov, A.; Pavlov, S.; Panarin, O.; Maliutin, A.; Rykovanov, S.; Fedorov, M. "Zhores"—Petaflops supercomputer for data-driven modeling, machine learning and artificial intelligence installed in Skolkovo Institute of Science and Technology. *Open Engineering* **2019**, *9*, 512–520.